Distributed Sensor Networks for Detection of Mobile Radioactive Sources

Robert J. Nemzek, Jared S. Dreicer, David C. Torney, and Tony T. Warnock

***Abstract*—The ability to track illicit radioactive transport through an urban environment has obvious national security applications. This goal may be achieved by means of individual portal monitors, or by a network of distributed sensors. We have examined the distributed sensing problem by modeling a network of scintillation detectors measuring a Cesium-137 source. We examine signal-to-noise behavior that arises in the simple combination of data from networked radiation sensors. We find that, in the ideal case, large increases in signal-to-noise compared to an individual detector can be achieved, even for a moving source. We also discuss statistical techniques for localizing and tracking single and multiple radioactive sources.**

***Index Terms*—Bayes procedures, coherent addition, counter-terrorism, signal detection and estimation, velocity measurement.**

I. Introduction

THE distributed sensor network project at Los Alamos National Laboratory is investigating the use of networked detection for various applications, including tracking of radioactive materials. Currently proposed solutions to the detection of radioactive materials in an urban setting typically involve the use of individual, large, portal-monitor-style detectors positioned at choke points. This may not ultimately be acceptable in an urban environment, given the large number of transport avenues to be covered and the potential objections to large detection packages; a more discreet solution may be required. We therefore are investigating the use of large numbers of small detectors. We are not attempting here to answer the question of whether detection limits, for example, are better or worse in such a situation, compared to a large-detector scenario. We are only examining the characteristics, specifically signal-to-noise ratio (SNR), to be expected in a distributed network. We assume that the detectors in our system are stand-alone and wirelessly networked to allow immediate data sharing with freedom from the need for an infrastructure (e.g., external power, cables, and internet connections). We furthermore assume that such a sensor network would be devised as an independent and fully distributed entity, not requiring a centralized processing station. This is achievable by using microcontrollers built into the individual sensing nodes or by incorporating dedicated processing nodes into the network, in cases where more processing power is required than can be conveniently fitted into the sensors themselves. The Distributed Sensor Network (DSN) then consists of a large number of small, simple, detector/processor nodes with the capability of sharing either raw or partially processed data. The data are autonomously analyzed by the network. This is done either by individual nodes collecting data (through some combination of automatic publishing and requesting) or through the use of a software agent traveling through the network, collecting relevant data, and calculating partial results *in situ*.

In addition to the radiation detectors themselves, the sensor nodes on the network would probably be equipped with GPS receivers for time synchronization and position information. A complete detection package could be built with sufficiently low power requirements to allow long-term operation on battery power. The addition of a solar recharge system would permit a system capable of long-term autonomous monitoring to be fielded on short notice, for example, at special events or in response to particular threats. Such a system would require *ad hoc* networking capabilities, as are being researched at a number of institutions. Finally, any deployed system would need mechanisms for tagging suspect vehicles (e.g., a triggered video system) and alerting authorities to a potential threat.

In this paper, we characterize the signal-to-noise envelope for this application of distributed networks. We also develop Bayesian methods for the estimation of radioactive source parameters, revealing trajectory and activity.

II. SNR for a Single Detector

Our chosen scenario: a radioactive source is traveling at constant speed parallel to a line of evenly spaced identical detectors. This is a simple setup, but it does represent an urban or roadside situation. We take the source to be a small quantity of Cesium-137; this isotope was chosen because its availability in industrial sources and its typical powdered form (as CsCl) make it a potential element of a radiological dispersal device ("dirty bomb"). The source is described by its speed, distance of closest approach to any particular detector, and activity. Any actual device being transported would have both intentional and intrinsic shielding; for convenience, we define the activity of the source to be its equivalent (in terms of number of gammas/s escaping the vehicle) in an unshielded condition. We choose as our detectors the ubiquitous 75-mm NaI scintillator. The source-to-detector response function in the model includes the inverse square fall-off, atmospheric attenuation, and factors for the capture and

Manuscript received October 21, 2003; revised April 18, 2004. This work was supported by the Department of Energy/NNSA and the Los Alamos National Laboratory Laboratory Directed Research and Development funds under the University of California Contract W-7405-ENG-36.

R. J. Nemzek is with the Los Alamos National Laboratory, ISR-4, MS-D448, Los Alamos, NM 87545 USA (e-mail: nemzek@lanl.gov).

J. S. Dreicer is with the Los Alamos National Laboratory, DIR, MS-D440, Los Alamos, NM 87545 USA (e-mail: jdreicer@lanl.gov).

D. C. Torney is with the Los Alamos National Laboratory, T-10, MS-K710, Los Alamos, NM 87545 USA (e-mail: dct@lanl.gov).

T. T. Warnock is with the Los Alamos National Laboratory, CCS-3, MS-B265, Los Alamos, NM 87545 USA (e-mail: ttw@lanl.gov).

Digital Object Identifier 10.1109/TNS.2004.832582

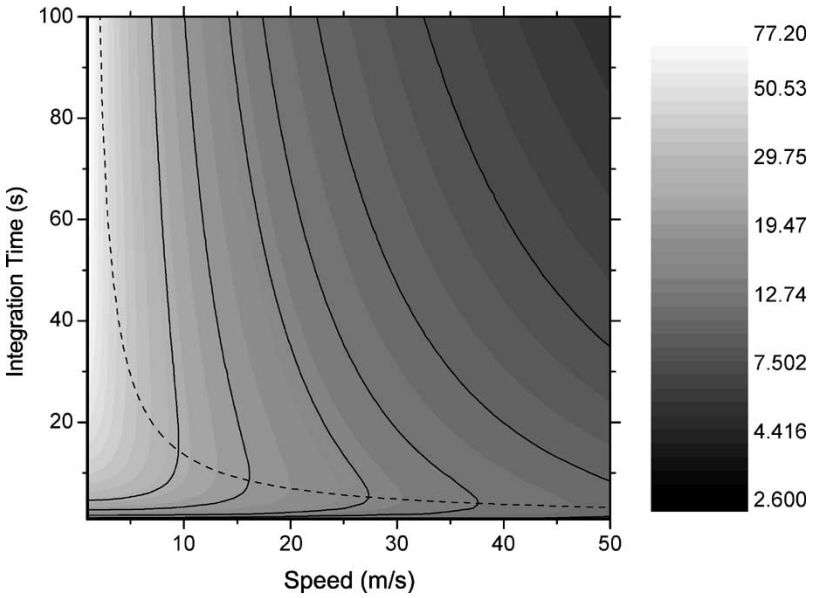

Fig. 1. SNR for a single detector; the distance of the closest approach is 20 m, the effective source activity is 0.01 C. Shading represents SNR, according to the color scale at right. Contour lines (solid) are at SNR values of 25, 20, 15, 12.5, 10, and 7.5 (left to right). The dotted line defines the (hyperbolic) locus of optimal integration times.

conversion in the NaI of gammas into pulses within the Cs-137 photopeak (662 keV). Edge effects, angular response, and any sources of electronic noise are ignored for the present, as we are most concerned with discovering the overall features of the SNR, rather than with calculating the exact SNR for a specific sensor. At the outset, we assume an array of 25 detectors in a straight, level line, with constant 10-m separation between individual detectors. Our interest here is not to determine the ultimate sensitivity of a fully realistic sensor network, but to learn the characteristics of a network in the presence of a moving source.

To calculate the SNR for a single detector, we start by calculating an "interaction length": the product of the source speed and the detector's integration time. We consider this interaction length to be centered on the detector. The source is then propagated from one end of the interaction length to the other at the chosen speed, and count rates are calculated and integrated in 10-ms bins for the duration of the integration time. We also include a constant background level β of 7 counts/s under the photopeak, a value derived from published natural background spectra [1]. SNR is then calculated as $(S/\sqrt{S+B})$, where S represents the integrated count rate from the source and B the integrated counts due to background. If background levels are varying, it may be appropriate to calculate SNR as simply $(S/(\sqrt{S}+B))$ [2], [3]. We have retained the standard definition, the difference being minor for the situations we are considering.

Ordinarily, the SNR would increase with the square root of the detector integration time. But this is not the case when considering a moving source. As the integration time increases, the source spends more and more time increasingly far from the detector, reducing the average count rate; the situation worsens as the speed of the source increases. Fig. 1, depicting the results of one set of our calculations, bears this out. In Fig. 1, shading indicates calculated SNR: white represents high SNR. As the speed of the source (horizontal axis) increases, the SNR always drops. As the integration time is increased (vertical axis), the SNR first increases, then drops, an effect most easily seen at moderately high source speeds. The net effect is that, for any given source speed, there is an integration time T that maximizes the SNR. This is clearly seen by examining the solid contour lines; the peak SNR for a given speed is at the "nose" of a contour. This result can also be derived by means of an analytical approximation; [4] used the expression

$$T = \frac{2.8h}{v}$$

where T is the integration time for maximum SNR, h is the distance of the closest approach, v is the source speed. Likewise, the locus of points of maximum SNR in Fig. 1, shown by the dotted curve, follows a vT hyperbola, with a coefficient of 12. A change in any of the parameters of our model (closest approach, source activity, detector type, background, gamma energy, and so on) would alter the specifics of the SNR curves from that demonstrated by Fig. 1, but the general behavior (maximum SNR at an integration time given by a hyperbolic curve) would remain the same, according to the following reasoning.

Assume that at $t = 0$ the source is at distance h from the sensor, that is

$$r^2(t) = h^2 + v^2t^2.$$

Therefore, assuming the count rate equals $\chi a/r^2$, where χ is a cross-section coefficient, and a the source activity, the instantaneous count rates at time t for signal and background, respectively, are

$$\frac{\chi a}{h^2 + v^2t^2}$$
$$\beta.$$

Setting these equal, using the positive root t' and noting $T = 2t'$, we have

$$T = \frac{2h}{v}\left(\frac{\chi a}{\beta h^2} - 1\right)^{\frac{1}{2}}, \qquad \chi a \geq \beta h^2$$
$$= 0, \qquad \text{otherwise.}$$

For fixed parameters, $vT = \text{constant}$, i.e., a hyperbola results. For the situation demonstrated in Fig. 1 (75 mm detector, 0.3 cm^{-1} detector attenuation coefficient, 0.49 photopeak fraction, 0.0001 cm^{-1} atmospheric attenuation coefficient, 20 m closest approach, and a 0.01 C source) the constant evaluates to 36, a factor of three greater than manifest by Fig. 1, whose simulation also includes factors for atmospheric attenuation, detector attenuation, and photopeak fraction.

III. SNR for Networked Detectors

Next we examine the increase in SNR made possible by adding together detector outputs. We make the assumption that all 25 detectors in the network are operating identically, with synchronized integration times and with identical background levels. One detector (the 13th or central unit) is treated as in the previous section, i.e., it is the detector on which the interaction length happens to be centered. The calculation of SNR for the surrounding detectors is performed as before, with the exception that the center of the interaction length is displaced some distance to one side or the other. We assume that the integrated counts from each detector are all made available at some point in the network. We then add the SNR values in quadrature for varying numbers of detectors: 1 (central detector), 3 (center plus one on each side), 5 (center plus two on each side), and so on, to a total of 25 detectors.

Typical results are shown in Fig. 2, expressed as a ratio of SNR for the combined detectors to SNR for a single detector. Fig. 2(a) is for a source speed of 20 m/s, while Fig. 2(b) is for a source speed of 10 m/s. Each curve on the plots represents a different integration time. For each integration time, the SNR ratio increases as the number of detectors increases. After some number of detectors is added, however, the SNR ratio curve flattens out. This occurs because the additional detectors are increasingly far from the interaction length of the source, and therefore the integrated background is relatively larger. As the interaction length is increased (compare curves at increasing integration times in either panel or the same integration time in both panels), the greater the number of detectors that can be added before the rolloff occurs. At the longest interaction lengths shown in Fig. 2(a) and (b) (integration times of 50 and 100 s), the SNR ratio curve collapses into a straight line (on our log–log plot) for all detector combinations. This line is simply the $\sqrt{N}$ (where N is the number of detectors) increase one would expect from the statistics of adding co-located detectors, i.e., the motion of the source combined with the integration time has made the detectors virtually co-located. The curves in Fig. 2 are symmetric with respect to integration time and speed; that is, the SNR ratio curve for a 1-s integration time and a source moving at 10 m/s is identical to the curve for a 10-s integration time and a 1 m/s source speed. Only their product, the interaction length, matters. In Fig. 2, the curves for higher speeds

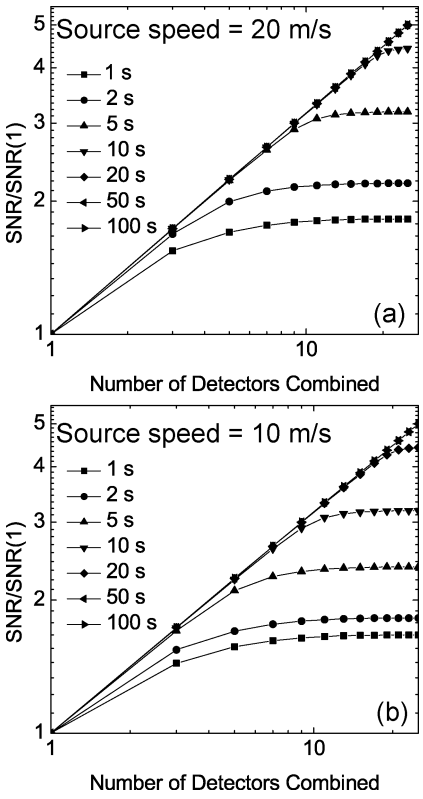

Fig. 2. SNR for multiple sensors ratioed to SNR for a single sensor. (a) Source moving at 20 m/s. (b) Source moving at 10 m/s. Effective source activity is 0.01 C and the distance of the closest approach is 20 m. Legends give the integration time for each curve.

are above those for lower speeds, at any given integration time. This does not contradict the results of the previous section that source speed reduces SNR, since Fig. 2 presents a ratio of SNRs. If absolute SNR values were plotted, the SNR for some number of combined detectors and a high-speed source would be lower than that for the same number of detectors and a low-speed source. Some situations might have a crossover where a curve that has leveled off intercepts one that is still increasing.

With a system of networked detectors capable of autonomous storage and trading of data, it is straightforward to do something more complicated than described in the previous paragraph: the coherent addition of data. By "coherent addition," we mean the combination of data values while taking into account the motion of the source: the counts from each detector are added together with increasing time lags, so that (hopefully) the integration window follows the source as it moves from detector to detector. We simulated this in our model by propagating the source past the detector array in a series of contiguous interaction lengths (again, we are assuming that the detectors are integrating in synchronization). We first selected the integration interval that provided the maximum SNR for the central (13th) detector in our array of 25. We then added detectors with zero lags (the same situation as in Fig. 2), one lag (nearest neighbors to the center are combined using the integration time one step ahead or behind the center, second nearest neighbors two steps ahead or behind, etc.), two lags (nearest neighbors two steps removed, second nearest neighbors four steps removed, etc.), and so on. Detectors are combined in groups totaling 1, 3, 5,. . .,

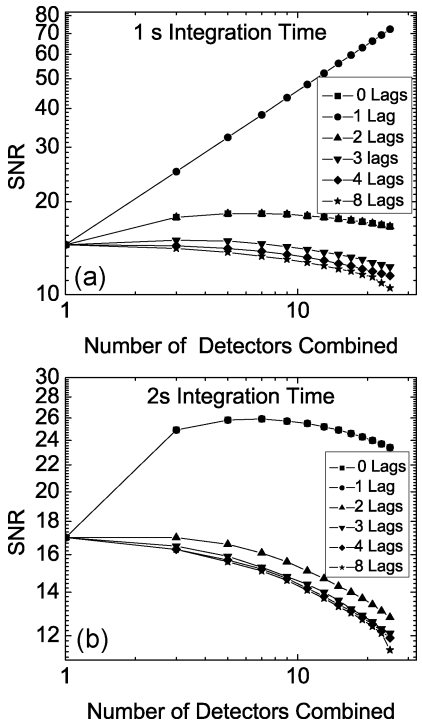

Fig. 3. SNR for detector outputs combined by coherent addition. (a) A 1-s integration time. (b) A 2-s integration time. For both panels, the source speed equals 10 m/s, the effective source activity equals 0.001 C, and the distance of the closest approach is 5 m. The legend gives the lag value for each curve.

25 as before. Again, the data values were added in quadrature and SNR calculated; the results are presented in Fig. 3. When the interaction length matches the detector spacing and number of lags [Fig. 3(a), one lag], the SNR increases along the $\sqrt{N}$ curve without limit. There is no rolloff as the number of detectors is increased, as the coherent addition process keeps the source centered on the integration time window of each detector. Under less favorable conditions,[(Fig. 3(b), one lag], the SNR increases with the combination of a few detectors and then rolls off. For very poor matches [Fig. 3(b), lags $=$3, 4, 5], the SNR for combined detectors is always worse than that of a single detector.

Finally, in Fig. 4, we see the effect of a varying speed on the coherent integration process. We start with a situation in which the lag factor is chosen to produce an exact match with the source speed, giving a linearly increasing SNR ratio on the log–log plot. As a small, constant acceleration is introduced (0.02 and 0.1 m/s^2 are shown), the SNR ratio begins to break away from the $\sqrt{N}$ curve, with the effect increasing as additional detectors are combined. The loss in SNR is approximately 50% for 25 detectors and an acceleration of 0.1 m/s^2. In this demonstration, the initial speed of the source was chosen so that the accelerating source was moving at 10 m/s as it passed the 25th detector in the array, after an elapsed time of 100 s.

While our signal-to-noise simulations demonstrate the measurement limitations that will ensue for the any detector network, they do not address the issue of characterizing a source based upon those measurements, which is the topic we address next. If we idealize the situation of our simulations by eliminating atmospheric attenuation, we can derive insights into our

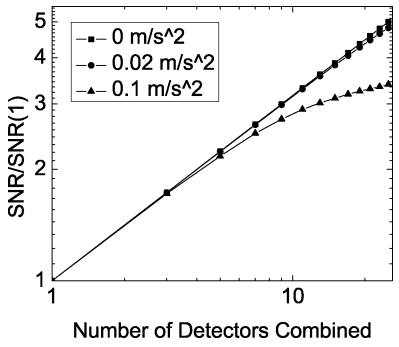

Fig. 4. SNR for detectors combined with coherent addition, including an acceleration term, ratioed to SNR for a single detector. Integration time equals 1 s, effective source activity equals 0.001 C, and the distance of the closest approach is 5 m. The initial source speed was chosen such that the source was traveling at 10 m/s as it passed the 25th detector in the array, after an elapsed time of 100 s. The legend gives the acceleration value for each curve.

problem analytically. In particular, if we have a source of activity a and a cross-section coefficient χ, the average number of recorded counts in the sensor can be expressed as $\chi a/r^2$, where r is the distance from source to sensor. If our network is a line of sensors equally spaced by distance d, and the source passes on a parallel line separated from the sensor array by a distance h, the average total count rate it induces, summed over all the sensors, is readily found to be

$$\frac{\pi\chi a}{dh}. \tag{1}$$

This result may be obtained from the formulas in the next section.

IV. Bayesian Methods for Radioactive-Source Localization

Localization of nonacoustic sources has been the subject of general investigations [5]. Here we elaborate Bayesian methods for the detection and characterization of mobile, radioactive sources as in [6], noting that Bayesian methods have been implemented for related objectives [7]–[9]. The limited amount of published work in this area belies its import for national security.

Although they cannot transcend the signal-to-noise envelope described above, the methods considered here may be construed as generalizing the aforesaid coherent addition of counts. For instance, only these generalizations anticipate sources subject to accelerations. Our methods provide not only estimates for source parameters but also respective confidence domains.

Recalling the foregoing, our sensors occur at intervals of length d on a line. Their number is Ψ, and they collect counts over successive time intervals of size τ. The level of background radiation is constant, with mean β counts per second. (Our methods will also readily accommodate variable backgrounds.) The source is assumed to move at constant speed v: parallel to the line of the sensors with separation $h > 0$. In addition to h and v, the source is characterized by its activity a, having dimensions T^{-1}; $a\tau$ for instance, equals the expected number of counts which would be captured in a time interval of length τ by a spherical, 100%-efficient sensor centered about

the source. Furthermore, the expected rate of count collection by a sensor is assumed to be proportional to the solid angle it subtends, taken to be isotropic (as previously mentioned). Our previous SNR calculations were based on a realistically modeled 75-mm NaI detector, but in the following sections, the detector is assumed to have physical dimensions of zero. The simulations are dimensionless, but we quote results for source speed and detector spacing using centimeters. In a fully realized simulation, the detectors would be of a specific size, spaced meters or perhaps tens of meters apart, and source speeds would be on the order of 10 m/s.

Our methods estimate a, h, and v, based upon the c_{st}'s: the counts recorded by sensor s in time interval t (of length τ), $s = 1, 2, \ldots, \Psi$, $t = 1, 2, \ldots, \Theta$. The key to our methods is a formula for the probability of the c_{st}'s in terms of β, d, τ, and the source parameters. We assume Poisson statistics obtain, and, consequently, the sought formula is

$$\Pr(c_{11}, c_{12}, \ldots, c_{\Psi\Theta} | a, h, v; \beta, d, \tau) = \prod_{s=1}^{\Psi} \prod_{t=1}^{\Theta} \exp\{-\mu_{st}\} \frac{\mu_{st}^{c_{st}}}{c_{st}!} \quad (2)$$

where μ_{st} denotes the expected number of counts recorded by sensor s during time interval t. To formulate the μ_{st}'s, we recall our approximation that the capture rates of the sensors equal $\chi a r_s^{-2}$, respectively, where χ is the cross-section coefficient and the activity of the source, with the distance between the sensor s and source equal to r_s. Therefore, the following integral measures the expected number of nonbackground counts recorded by sensor s in time interval t

$$\frac{\chi a}{hv} \int_{x_{st}}^{x_{st}+v\tau} \frac{dx}{r_s^2(x)} \quad (3)$$

where x_{st} denotes the coordinate of the source at the beginning of the tth time interval—along the line of the sensors, with origin at the position of sensor s and increasing in the direction of motion and where $r_s(x)$ denotes the distance from x to sensor s. It follows that

$$\mu_{st} = \frac{\chi a}{hv} \left\{ \tan^{-1}\left(\frac{(x_{st} + v\tau)}{h}\right) - \tan^{-1}\left(\frac{x_{st}}{h}\right) \right\} + \beta\tau, \quad s = 1, 2, \ldots, \Psi, \quad t = 1, 2, \ldots, \Theta. \quad (4)$$

The range of these arctangents is $[-\pi/2, \pi/2)$; monotonicity guarantees nonnegativity of the μ_{st}'s, which are to be substituted into (2).

We assume that β, d, and τ are given constants. Equation (2), along with a suitable prior distribution, specifies a posterior distribution on (a, h, v), given the data. This distribution may be characterized through its *moments*, which, based on a uniform prior, are defined as given in (5), shown at the bottom of page, where a_m, h_m, and v_m denote respective upper bounds. In particular, the "first moments," $\langle a \rangle$, $\langle h \rangle$, and $\langle v \rangle$, are our estimates for the source parameters, and the second moments may be used to obtain an ellipsoidal confidence domain, whose volume may be estimated from the eigenvalues of the matrix of second moments: through the reciprocal of their product.

More realistic geometric models for the cross section could be incorporated, yielding a formula analogous to (4). For instance, were the sensor a rectangle with base of length l, lying in the line of sensors, then, with the source at x (coordinate as above), the solid angle would, in a far-field approximation, be reduced from $\chi a r_s^{-2}(x)$ by a factor of $\sin\theta$, where θ denotes either of the supplementary angles between the ray through the source from the center of the base of the sensor and the line of sensors. The integral to be substituted for (3) into (4) evaluates to

$$\left. \frac{\chi a \xi}{hv\sqrt{1+\xi^2}} \right|_{\xi=x_{st}}^{\xi=x_{st}+v\tau}.$$

It follows that the analog of (1) has a rate reduced by a factor of $2/\pi$.

V. Implementation

Adaptive Gaussian quadrature may be used to evaluate the integrals of (5)—which yield our parameter estimates. We chose, instead, to implement uniform sampling of $[0, a_m) \times [0, h_m) \times [0, v_m)$ (and respective function evaluation) because this approach was effective for the minute integrands engenderable by (2), as will be seen. This sampling is achievable using either triples of pseudorandom numbers or low-discrepancy collections of points, with the latter affording asymptotically arbitrarily greater accuracy for the same computational cost [10], [11]. It may be noted that "importance sampling" could yield further improvement.

The sums resulting from such sampling afford approximations to the integrals. To avoid underflow, the logarithm of the sum was used, and precautions were implemented to mitigate roundoff in the generation of partial sums. To reduce the fluctuations in these approximations, the same points were used for all the moments computed: the zeroth [*viz.* the denominator of (5)] through the second.

VI. Simulations

Our motivation for performing these simulations was to determine the capabilities and limitations of our Bayesian methods—for sensor-network data. With exceptions as noted, simulations involved ten sensors. The integration time (the

$$\langle a^i h^j v^k \rangle \stackrel{def}{=} \frac{\int_0^{a_m} \int_0^{h_m} \int_0^{v_m} a^i h^j v^k \Pr(c_{11}, c_{12}, \ldots, c_{\Psi\Theta} | a, h, v; \beta, d, \tau) da dh dv}{\int_0^{a_m} \int_0^{h_m} \int_0^{v_m} \Pr(c_{11}, c_{12}, \ldots, c_{\Psi\Theta} | a, h, v; \beta, d, \tau) da dh dv} \quad (5)$$

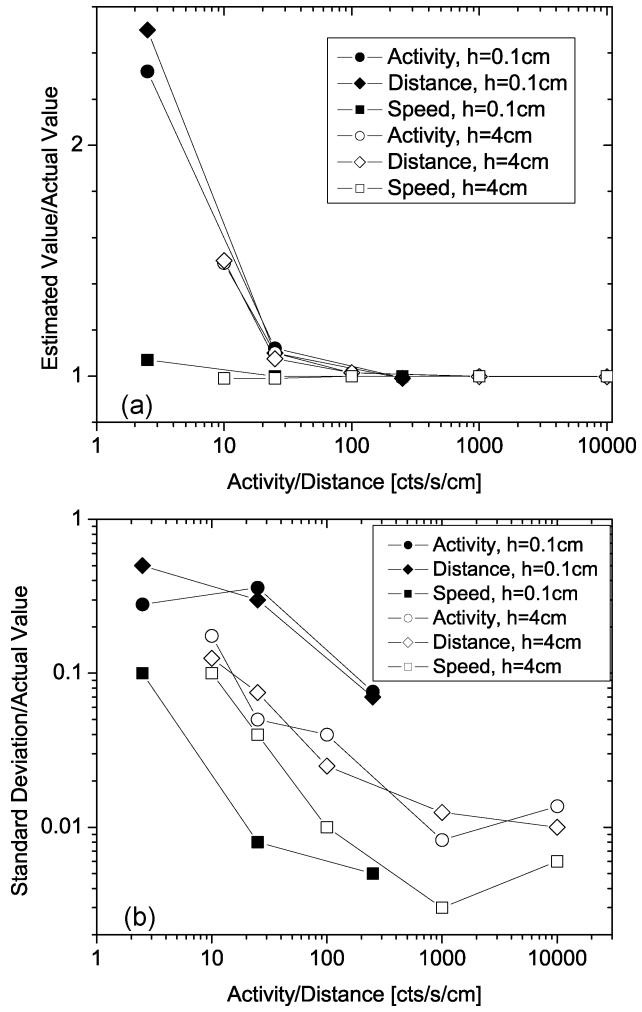

Fig. 5. Noise limitations ($\beta = 7$ cts/s, $d = 4$ cm, $v = 1$ cm/s, number of sensors $= 10$, $\tau = 2$ s, number of time points $= 21$, $h = 0.1$ cm or 4 cm, as indicated in legend). (a) $\langle a \rangle / a$, $\langle h \rangle / h$, and $\langle v \rangle / v$, plotted as a function of a/h. The average first moments are plotted, after five realizations of Poisson random variables with the same expectations—for each time interval and each sensor. (b) The standard deviations of the first moments over the five realizations are plotted, after normalizing by the parameter value, as in (a).

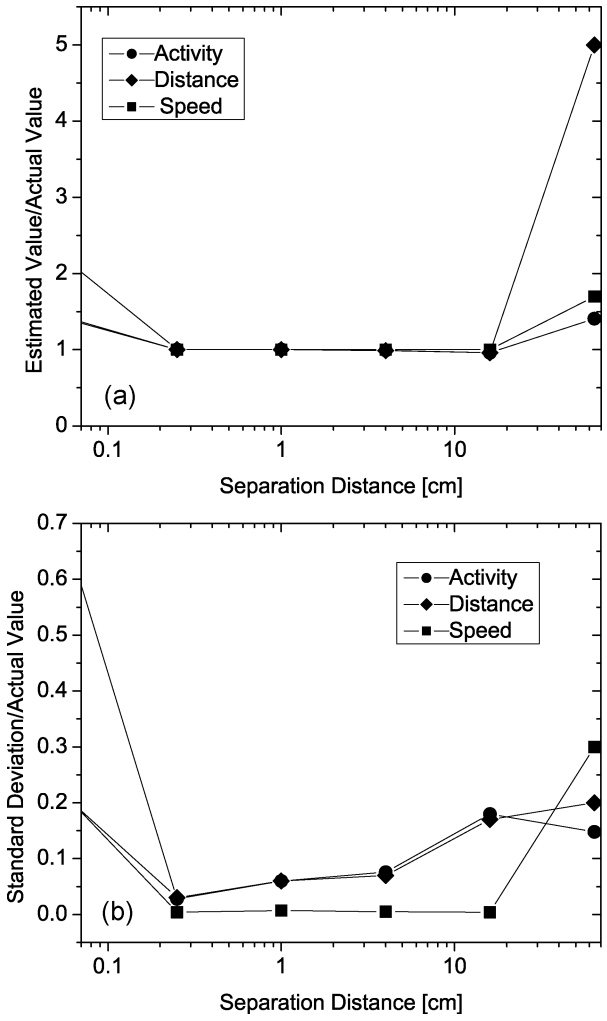

Fig. 6. Varying the array length relative to the distance traversed by the source. (a) and (b) are the normalized parameter estimates and their standard deviations, respectively, as described in the legend of Fig. 5. $\beta = 7$ cts/s, $\tau = 2$ s, $v = 1$ cm/s, number of sensors $= 10$, number of time points $= 21$, $h = 0.1$ cm, d ranges from 1/16 to 64 cm. The distance traversed by the source $= 42$ cm. The length of the array varies from 9/16 to 576 cm, respectively.

length of the time interval over which sensors collect counts) was two seconds, and the number of time intervals was 21. At the middle of the 11th interval, the source was taken to be opposite the middle of the segment of sensors. Five repetitions, with independently chosen Poisson counts, were used, and the average and the square root of the variance (referred to as the standard deviation) of the first moments $\langle a \rangle$, $\langle h \rangle$, and $\langle v \rangle$ are reported. For simplicity, $\chi = 1$.

We usually estimated the moments using 2^{24} random triples. The errors of these estimates contributed to the standard deviations. Smaller numbers of low-discrepancy points [11] yielded similar accuracy, as will be seen. We chose upper bounds for integration which were an order of magnitude larger than the respective true parameter value. Note that in our simulations the failure to obtain a reliable estimate for any of the parameters is indicated by the estimate being close to the midpoint of the respective integration interval.

Fig. 5(a) and (b) illustrates the dependence of the parameter estimates and their accuracy upon a/h. For $50 < a/h$, all parameters are well estimated. For $2 < a/h < 10$, only $\langle v \rangle$ is well estimated. Also, if $a/h < 2$, all parameters are poorly estimated. This is consistent with (1), which indicates that the sum of the signals should depend, roughly, on a/h. Here, the coefficient is roughly unity because $d = 4$. As $\beta = 7$, we would expect to be able to characterize sources with $10 < a/h$. Fig. 5(b) depicts the increase in the noise in the parameter estimates with decreasing a/h.

Fig. 6(a) and (b) depicts the accuracy in the parameter estimates as the length of the array of sensors varies relative to the length of the source's trajectory. The best estimates occur when the lengths are comparable. Poor estimates are obtained at both extremes: when the trajectory is much shorter or much longer than the interval containing the sensors.

Fig. 7(a) and (b) illustrates the degradation in parameter estimates as the source speed is increased and the spacing between sensors increased proportionately. Here, this degradation is significant when $10 \leq v$, disproportionate to what is expected based on (1) and to that manifest in Fig. 5(a).

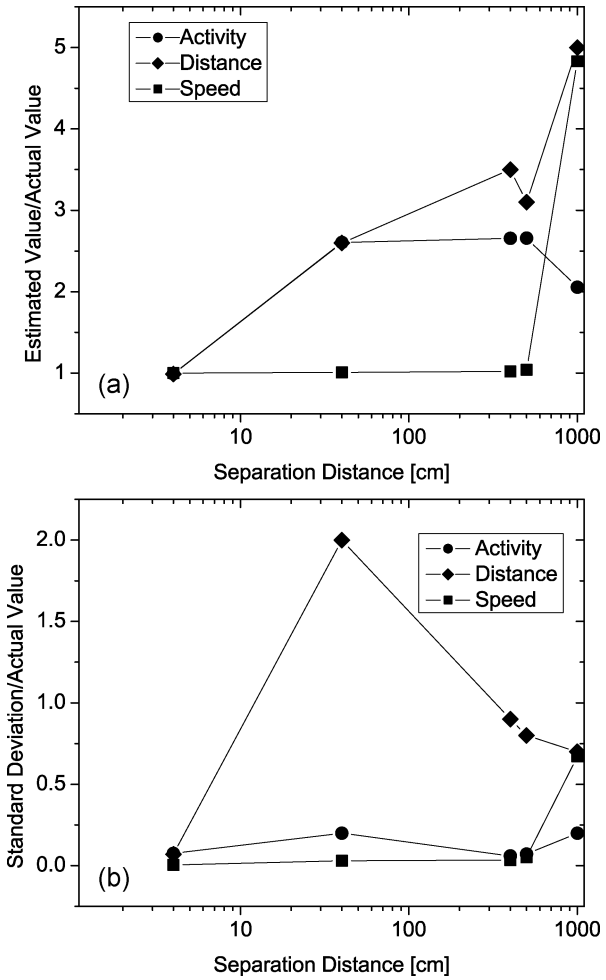

Fig. 7. Consequences of sparse measurements. (a), (b) The normalized parameter estimates and their standard deviations, respectively, as described in the legend of Fig. 5. Here, $\beta = 7$ cts/s, $\tau = 2$ s, number of sensors $= 10$, number of time points $= 21$, $h = 0.1$ cm. d ranges from 4 to 1000 cm, and $v = d/4$ cm/s.

Our methods are applicable in situations broader than we have demonstrated so far. As an illustration, we let the location of the source at time zero x_0 be a random position within the array, rather than its midpoint. Then the four-dimensional analog of (5) can be used to estimate a, h, v, and x_0. For comparison, in Table I, we report respective estimates of $\langle a \rangle$, $\langle h \rangle$, and $\langle v \rangle$. Using the parameters listed in the table caption, good estimates were obtained using (5).

Table II demonstrates the advantageousness of increasing the number of sensors. For all parameters, as the number of sensors is increased (first column), the normalized standard deviation decreases.

Table III compares the efficacies of two methods of sampling points—pseudorandom triples and low-discrepancy—for evaluating the integrals of (5). It may be seen that an order of magnitude fewer "low-discrepancy points" yields comparable accuracy. Note also that the improvement in accuracy when the number of pseudorandom points is increased by a factor of 64 is about 5/3. Thus, the empirical behavior of the variance in the parameter estimates is the inverse fourth root of the number of such points, which is a weaker dependence than afforded by better behaved integrands. Poisson fluctuations also contribute to these estimates: contributions whose magnitudes have yet to be determined.

TABLE I
PARAMETER ESTIMATES FOR A RANDOM INITIAL SOURCE POSITION

# Integration Points	<a>	<h>	<v>
2^{20}	56 +/- 26	0.22 +/- 0.1	1.00 +/- 0.01
2^{24}	32 +/- 11	0.13 +/- 0.05	1.00 +/- 0.01
2^{28}	23.7 +/- 6.8	0.09 +/- 0.03	1.00 +/- 0.003

Number of sensors $= 10$, spacing $= 4$ cm, number of time points $= 10$, $\beta = 7$ cts/s, $\tau = 2$ s, $v = 1$ cm/s, $h = 0.1$ cm, $a = 25$ cts/s

TABLE II
INCREASING THE NUMBER OF SENSORS

Ψ	<a>/a	σ(a)/a	<h>/h	σ(h)/h	<v>/v	σ(v)/v
5	1.024	0.132	1.00	0.10	1.00	0.005
10	0.992	0.076	0.99	0.07	1.00	0.005
40	1.028	0.050	1.00	0.05	1.00	0.001

Number of time points $= 21$, $\beta = 7$ cts/s, $\tau = 2$ s, $v = 1$ cm/s, $h = 0.1$ cm, $a = 25$ cts/s. Increasing the number of sensors Ψ is given in column 1 with $d = 8, 4,$ and 1 for the three numbers of sensors.

TABLE III
COMPARISON OF SAMPLING TECHNIQUES. ACCURACY AS A FUNCTION OF THE NUMBER OF POINTS SAMPLED USING DIFFERENT METHODS FOR SELECTING POINTS: EITHER PSEUDORANDOM NUMBER TRIPLES, UNIFORM ON THE RECTANGULAR PARALLELEPIPED (PRT); OR LOW-DISCREPANCY POINTS (LD)[11]

Method	σ(a)	σ(h)	σ(v)	# Points
PRT	0.991	0.00402	0.00904	2^{21}
LD	0.848	0.00340	0.00502	2^{21}
PRT	0.905	0.00389	0.00655	2^{24}
LD	0.800	0.00325	0.00497	2^{24}
PRT	0.681	0.00273	0.00505	2^{27}

VII. CONCLUSION

The SNR that can be expected from a single detector measuring a moving source is considerably different from what is expected for a stationary source: there is an optimal integration time which is proportional to the ratio of closest-approach distance to source speed. When combining readings of a moving source from an array of detectors, we find that SNR increases along a $\sqrt{N}$ curve for small numbers of detectors, but levels off for larger numbers of detectors, with the position of the roll-off depending on the "interaction length," given by the product of source speed and integration time. This limitation can be overcome by incorporating appropriate time lags into the addition, such that the integration windows used in the addition follows the source as it moves from detector to detector.

A small detector will always have lower efficiency than a large detector, although in the presence of background the two may be equivalent in detection abilities [3]. For a detector array, the coherent addition process can make up for the low efficiency of small detectors. The difficulty, of course, is that the sensor network must have some knowledge of the traffic speed to determine the appropriate time lag for addition. The sensor network design could easily incorporate an average speed measurement, or even a vehicle-specific speed in areas of low traffic density. Alternatively, if the traffic speed is relatively constant, the sensor

network's data fusion algorithm could simply step through different lag values; as Fig. 3 demonstrates, there will be a relatively limited set of reasonable values, and a rapid improvement in SNR at the correct one. In any event, the increasing SNR shown in Fig. 3 would not be sustained indefinitely in a real-world situation.

An actual urban or roadside situation is a two-dimensional (2-D) problem. However, it can be considered an assemblage of one-dimensional paths: blocks. Our simulations are equivalent to sensor network processing on a block-by-block basis. A full simulation, including sources passing potential cross streets, is a much more difficult problem. On the other hand, our results show that, in the absence of perfect knowledge of source speed, the gains to be had by adding sensors will level off after some number of sensors, simplifying the full 2-D problem. This limitation also introduces the argument that individual portal monitors may be equivalent to, or better than, networked sensors. However, as stated earlier, portal monitors may be objectionable compared to small networked sensors. Also, the urban environment is defined by obstruction, which may make multiple sensors more likely to have a clear view of a source. Obviously, determining the combination algorithm for a congested area could be quite difficult. The advantages offered by sensor networks over portals include the ability to make more precise estimates, for instance, of the trajectory of a radioactive source. Note that the applicability of coherent addition extends to trajectories involving accelerations, with the requirement that the trajectory be known (for example, if a single vehicle is present and the DSN is equipped with radar or some other speed/position sensor). Ambiguity in the trajectory of a candidate source is addressed by Bayesian methods, which provide estimates of both the source characteristics and its trajectory.

For the most part, we did not also estimate the "time of arrival" of the source, avoiding this importunity by assuming knowledge of the time at which the source passes the midpoint of the segment containing the sensors. Although the problem we solve is, therefore, idealized, straightforward extension of our methods will be practical for estimation of this and additional parameters, as illustrated in Table I. An extension of our methods for sensors which capture an energy spectrum is immediate. With Bayesian methods, one must specify the characteristics of radiation sources of interest. Furthermore, one may view the problem of detection of constant-speed radioactive sources as a special case: in which one must integrate (2) over a domain in a, h, and v.

A common feature of the simulations is that, as the difficulty of estimation is increased, the errors in the estimates are most pronounced for $\langle a \rangle$ and $\langle h \rangle$. It is desirable to find mitigating methodologies, achieving uniform accuracy for all estimates.

Were there multiple sources, one would face the additional challenge of "partitioning" the counts at the sensors in order to make effective estimates for all of their parameters. It seems that importance sampling of "good" partitions would be a necessary component of effective methods for this problem [12]. In any case, the partitioning would occur atop methods similar to those elaborated above which could be applied to the individual sources based on a postulated "partition."

The coherent addition process is straightforward and well within the processing and data storage capabilities of simple distributed sensor systems. A system incorporating Bayesian methods may require the addition of dedicated processing nodes to provide the computational power needed for a timely decision. Performance tradeoffs, such as between sensitivity and computational requirements, remain to be evaluated. The ability to efficiently evaluate Bayesian integrals, as addressed by Table III, will be essential for addressing more complicated trajectories, which may necessitate further adaptations, involving importance sampling. The results shown here demonstrate that the system design for a radioactivity-detecting DSN will have clear imperatives for at least two important parameters: the integration time for a single detector and the maximum number of detector outputs that need to be combined at any one location. In an operational system, both of these quantities may have to be adaptive, as they depend on the speed of the source being detected.

REFERENCES

[1] R. R. Finck, K. Liden, and R. B. R. Persson, "In situ measurements of environmental gamma-radiation by use of a Ge(Li) spectrometer," *Nucl. Intrum. Methods*, vol. 135, pp. 559–567, May 1976.

[2] G. F. Knoll, *Radiation Detection and Measurement*, 3rd ed. New York: Wiley, 2000, pp. 785–787.

[3] K. P. Ziock and W. H. Goldstein, "The lost source, varying backgrounds and why bigger may not be better," in *Unattended Radiation Sensor Systems for Remote Applications*, J. I. Trombkar, Ed. New York: Amer. Inst. of Physics, 2002, pp. 60–70.

[4] G. M. Worth, C. N. Henry, R. D. Hastings, and S. W. France, "A Portable Gamma-Ray Detection System for Location of Radioactive Sources," Los Alamos National Laboratory, Los Alamos, NM, Tech. Rep. LA-UR-76-1241, Jun. 1976.

[5] A. B. Gershman and V. I. Turchin, "Nonwave field processing using sensor array approach," *Signal Processing*, vol. 44, pp. 197–210, Jun. 1995.

[6] M. Nelson and B. Rooney, "Final Review of the Arrayed Vehicle Monitor TI Proposal," Los Alamos National Laboratory, Los Alamos, NM, Tech. Rep. LA-UR-03-8055, Oct. 2003.

[7] C. T. Cunningham, "Detection and Tracking of a Stochastic Target Using Multiple Measurements," Lawrence Livermore National Laboratory, Livermore, CA, Tech. Rep. UCRL-ID-122 786, Nov. 1995.

[8] ——, "Bayesian Spectroscopy and Target Tracking," Lawrence Livermore National Laboratory, Livermore, CA, Tech. Rep. UCRL-143 305, May 2001.

[9] L. D. Stone, T. L. Corwin, and C. A. Barlow, *Bayesian Multiple Target Tracking*. Norwood, MA: Artech House, 1999, pp. 105–113.

[10] E. Novak and K. Ritter, "High dimensional integration of smooth functions over cubes," *Numerische Mathematik*, vol. 75, pp. 79–97, Nov. 1996.

[11] T. Warnock, "Effective Error Estimates for Quasi-Monte-Carlo Computations," Los Alamos National Laboratory, Los Alamos, NM, Tech. Rep. LA-UR-01-1950, 2001.

[12] E. Knill, A. Schliep, and D. C. Torney, "Interpretation of pooling experiments for screening a clone map," *J. Comp. Biol.*, vol. 3, pp. 395–406, Fall 1996.